



UNIVERSITÀ
DEGLI STUDI
FIRENZE

FLORE

Repository istituzionale dell'Università degli Studi di Firenze

Coronal heating in coupled photosphere-chromosphere-coronal systems: turbulence and leakage

Questa è la Versione finale referata (Post print/Accepted manuscript) della seguente pubblicazione:

Original Citation:

Coronal heating in coupled photosphere-chromosphere-coronal systems: turbulence and leakage / A. Verdini; R. Grappin; M. Velli. - In: ASTRONOMY & ASTROPHYSICS. - ISSN 0004-6361. - STAMPA. - 538:(2012), pp. A70-A77. [10.1051/0004-6361/201118046]

Availability:

The webpage <https://hdl.handle.net/2158/781740> of the repository was last updated on 2019-07-17T16:22:56Z

Published version:

DOI: 10.1051/0004-6361/201118046

Terms of use:

Open Access

La pubblicazione è resa disponibile sotto le norme e i termini della licenza di deposito, secondo quanto stabilito dalla Policy per l'accesso aperto dell'Università degli Studi di Firenze (<https://www.sba.unifi.it/upload/policy-oa-2016-1.pdf>)

Publisher copyright claim:

La data sopra indicata si riferisce all'ultimo aggiornamento della scheda del Repository FloRe - The above-mentioned date refers to the last update of the record in the Institutional Repository FloRe

(Article begins on next page)

Coronal heating in coupled photosphere-chromosphere-coronal systems: turbulence and leakage

A. Verdini¹, R. Grappin^{2,3}, and M. Velli⁴

¹ Solar-Terrestrial Center of Excellence – SIDC, Royal Observatory of Belgium, Bruxelles, Belgium
 e-mail: verdini@oma.be

² LUTH, Observatoire de Paris, Meudon, France

³ LPP, École Polytechnique, Palaiseau, France

⁴ JPL, California Institute of Technology, Pasadena, USA

Received 7 September 2011 / Accepted 16 November 2011

ABSTRACT

Context. Coronal loops act as resonant cavities for low-frequency fluctuations that are transmitted from the deeper layers of the solar atmosphere. These fluctuations are amplified in the corona and lead to the development of turbulence that in turn is able to dissipate the accumulated energy, thus heating the corona. However, trapping is not perfect, because some energy leaks down to the chromosphere on a long timescale, limiting the turbulent heating.

Aims. We consider the combined effects of turbulence and energy leakage from the corona to the photosphere in determining the turbulent energy level and associated heating rate in models of coronal loops, which include the chromosphere and transition region.

Methods. We use a piece-wise constant model for the Alfvén speed in loops and a reduced MHD-shell model to describe the interplay between turbulent dynamics in the direction perpendicular to the mean field and propagation along the field. Turbulence is sustained by incoming fluctuations that are equivalent, in the line-tied case, to forcing by the photospheric shear flows. While varying the turbulence strength, we systematically compare the average coronal energy level and dissipation in three models with increasing complexity: the classical closed model, the open corona, and the open corona including chromosphere (or three-layer model), with the last two models allowing energy leakage.

Results. We find that (i) leakage always plays a role. Even for strong turbulence, the dissipation time never becomes much lower than the leakage time, at least in the three-layer model; therefore, both the energy and the dissipation levels are systematically lower than in the line-tied model; (ii) in all models, the energy level is close to the resonant prediction, i.e., assuming an effective turbulent correlation time longer than the Alfvén coronal crossing time; (iii) the heating rate is close to the value given by the ratio of photospheric energy divided by the Alfvén crossing time; (iv) the coronal spectral range is divided in two: an inertial range with 5/3 spectral slope, and a large-scale peak where nonlinear couplings are inhibited by trapped resonant modes; (v) in the realistic three-layer model, the two-component spectrum leads to a global decrease in damping equal to Kolmogorov damping reduced by a factor u_{rms}/V_a^c where V_a^c is the coronal Alfvén speed.

Key words. methods: numerical – Sun: corona – magnetohydrodynamics (MHD) – turbulence – Sun: transition region – waves

1. Introduction

Solving the coronal heating problem involves understanding how fast magnetic energy can be accumulated in the corona and how fast this energy is dissipated. We investigate this problem by considering a model loop in which kinetic and magnetic energies are injected into the corona in the form of Alfvén waves generated by photospheric motions. A large body of work has been devoted to this problem (Milano et al. 1997; Dmitruk et al. 2003; Rappazzo et al. 2007, 2008; Nigro et al. 2004, 2005, 2008; Buchlin & Velli 2007). We consider here a previously neglected effect that plays a large role in regulating the turbulent energy balance in the corona, namely the leakage of coronal energy back down to the photosphere.

A solar loop can be described as a bundle of magnetic field lines that expand into the corona but are rooted in the denser photosphere at two (distant) points, so that their length is typically much greater than the transverse scale. The magnetic field is therefore mostly along the direction of the loop, and provided the transverse magnetic field is not too strong, the curvature of the loop may be neglected. In addition, if the ratio of the plasma

to magnetic field pressures is low, the motions are predominantly incompressible, so the transverse structure in density may be neglected compared to the gravitational stratification, while the expansion of the field from the denser layers of the photosphere and chromosphere into the corona may be taken into account via gradients along the field of the Alfvén speed. The resulting, simplified coronal loop retains the basic ingredients that lead to heating: turbulent coupling and propagation through a stratified atmosphere where stratification appears as an increase in the Alfvén speed from photosphere to corona.

The stratification is characterized by the ratio of mean Alfvén speeds in the photosphere (V_a^0) and in the corona (V_a^c), which is a small parameter:

$$\epsilon = V_a^0/V_a^c \ll 1. \quad (1)$$

The part of the wave spectrum entering the corona that we consider here is the low-frequency part, for which the Alfvén speed contrast is seen by waves of frequency ω as a sharp transition. This occurs if

$$\omega \lesssim \max(|\nabla V_a|) \approx (V_a^c - V_a^0)/H \approx 5\text{--}10 \text{ Hz} \quad (2)$$

for $V_a^c \approx 2000 \text{ km s}^{-1}$ and a transition region thickness of about $H = 200 \text{ km}$. For these low frequencies, the transition region (T.R.) acts as a transmitting and reflecting barrier, with the important property that the transmission is not symmetric, so that a coronal loop acts as a cavity that resonates at specific frequencies, based on the Alfvén crossing time $t_a^c = L_c/V_a^c$ (L_c is the length of the coronal part of loop):

$$\omega = n\pi V_a^c/L_c = n\pi/t_a^c \quad (3)$$

with $n = 0, 1, \dots$ (Ionson 1982; Hollweg 1984).

The cavity is perfectly insulated within the limit of infinite Alfvén speed contrast, i.e. $\epsilon = 0$, which corresponds to the so-called line-tied limit. In this limit, the corona exerts no feedback on the solar surface. The zero-frequency resonance is clearly distinct from the finite frequency resonances; in the former, the coronal magnetic energy grows without bounds, while the kinetic energy remains finite (Parker 1972; Rappazzo et al. 2007). In the latter case, both magnetic and kinetic coronal energies grow at equipartition.

In reality, the trapped energy is limited, because the cavity loses energy by two different mechanisms: damping (turbulent or not), and leakage owing to the finite Alfvén speed contrast. The leakage time is given by (Hollweg 1984; Ofman 2002; Grappin et al. 2008):

$$t_L = L_c/V_a^0. \quad (4)$$

The leakage time is much greater than the Alfvén crossing time, since $t_a^c = \epsilon t_L^1$. The dissipation rate of the loop will thus depend on (i) the energy input into the corona, as well as its frequency distribution (resonant or not), (ii) the part of the energy input that goes into heat and the part that returns to the solar surface (leakage).

In the previous works starting with Hollweg (1984), it has always been assumed that the leakage time was long compared to the (turbulent) dissipation time, so they neglected leakage (line-tied limit). Because neglecting leakage implies neglecting the back reaction of the corona on the deeper layers, in the line-tied limit the velocity can be imposed at the coronal base. This is justified if the leakage time is longer than the coronal dissipation time. Estimating the latter to be given by the photospheric turnover time $t_{NL}^0 = l_\perp/(2\pi U_0)$, we have for the ratio of the two timescales:

$$\chi_L = t_L/t_{NL}^0 \simeq (L/l_\perp)2\pi(U_0/V_a^0) \gtrsim 2\pi. \quad (5)$$

Since the coronal energy per unit mass is expected to reach higher values than at the surface, this largely justifies neglecting leakage. However, identifying the dissipation time with the turnover time might be erroneous, because turbulence, at least in some simulations (e.g., Nigro et al. 2008), shows a high degree of intermittency, so that the dissipation time is orders of magnitude longer than such simple estimates.

This motivates us to relax the line-tied hypothesis, using models of turbulent loops that include leakage. The problem then becomes more complex, since the velocity boundary conditions are no longer fixed, because the velocity is the sum of the incoming coronal base field and the outgoing coronal signal. We consider two versions of the problem that includes leakage. In the first version, which is called the one-layer model, we simply

¹ As seen in Sect. 2.3.3, Eq. (25), at every reflection a fraction ϵ of the coronal energy leaks from the transition region down to the chromosphere, so one needs $1/\epsilon$ reflections to evacuate the coronal energy, i.e. a timescale t_a^c/ϵ .

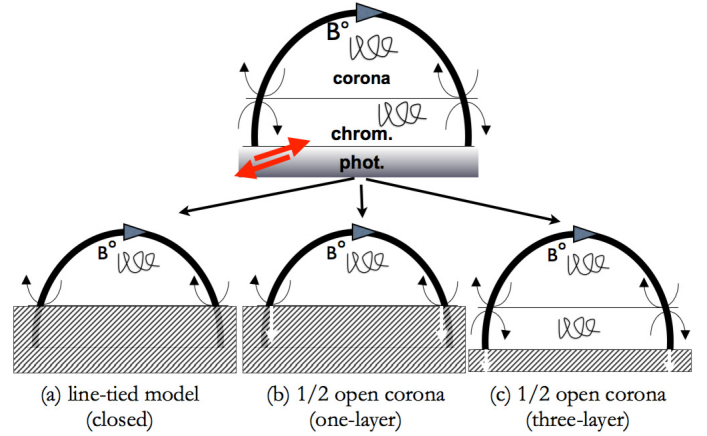


Fig. 1. Sketch of the coronal heating process. *Above:* the general problem of photospheric injection, transmission, turbulent dissipation, and leakage back to the photosphere. Red thick arrows at the left foot point represent the surface shear forcing. *Below:* the three numerical models considered in this paper: **a)** closed model (no leakage) with imposed velocity at the coronal base, **b)** semi-transparent corona with imposed wave input at the coronal base, **c)** semi-transparent corona including chromospheric turbulence with imposed wave input at the chromospheric base. Thin arrows indicate the wave reflection and transmission, white thick arrows represent the leakage out of the numerical domain.

change the boundary conditions at the coronal base, taking leakage into account. The incoming spectrum partly depends on the (given) signal assumed given by the chromospheric layers below and partly on the signal propagating downward from the corona and largely (but not fully) reflected. In the second version, which is called the three-layer model, the domain is enlarged to include two chromospheric layers. In that case, the signal propagating upward from the coronal base is still more uncontrolled than in the previous case, because the chromospheric turbulence that develops and determines the state of the coronal base is not directly predictable from the photospheric input. Figure 1 summarizes the models: the classical closed model, and the two versions including leakage.

To describe the turbulence dynamics along the loop, we use the shell model for reduced MHD (Nigro et al. 2005; Buchlin & Velli 2007). Shell models of turbulence share with full turbulence power-law energy spectra, as well as chaotic (intermittency) properties that are very close to direct numerical simulations of primitive MHD equations (Gloaguen et al. 1985; Biskamp 1994). The system is forced by introducing DC fluctuations, i.e., a spectrum of fluctuations at different perpendicular scales that is constant in time.

We show that the finite leakage time leads to significant differences with previous results obtained using line-tied boundary conditions. The plan is the following. The next section deals with basic physics, model equations, and parameters. Section three deals with simple phenomenology. Results are given in section four and section five contains the discussion.

2. Basic physics, model equations, and parameters

2.1. Three-layer atmosphere: linear reflection/transmission laws

We begin by describing our model atmosphere and the properties of linear Alfvén wave propagation within such an atmosphere. The atmosphere is considered to be stratified in the

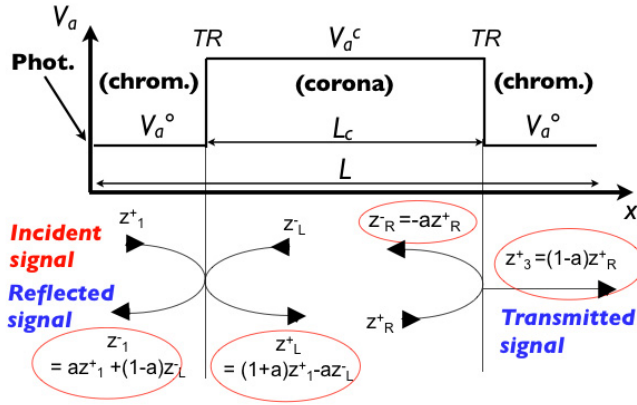


Fig. 2. The three-layer model: sketch of the transmission and reflection properties of transverse fluctuations at the coronal bases of a magnetic loop with piece-wise constant Alfvén speed, in the particular case considered here (no input from right chromosphere).

vertical direction, with three successive layers representing a left photosphere/chromosphere, the corona, and a right photosphere/chromosphere. The atmosphere is threaded by a vertical uniform field B_0 along which Alfvén waves propagate. In each of these three layers, the Alfvén speed is constant, so that a progressive Alfvén wave propagates at constant speed without deformation. When a wave encounters a density jump interface, the velocity and magnetic field fluctuations, which are parallel to the interface, are continuous. The proper Alfvén modes propagating in opposite directions along the loop are defined by the Elsässer variables:

$$z^\pm = u \mp b/\sqrt{\rho} \quad (6)$$

where ρ is the density and u, b are the velocity and magnetic field fluctuations, which are in planes parallel to the photosphere/corona transition region. Assuming a positive mean field B_0 , the quantity z^+ will propagate to the right and the quantity z^- to the left. It is immediately seen from this definition that the density jump at the transition region will determine a wave amplitude jump of the order of $1/\sqrt{\rho} = 1/\epsilon$. The derivation of the jump relations may be found in [Hollweg \(1984\)](#). Continuity of the velocity and magnetic field fluctuations at the two interfaces imply the following relations between wave amplitudes respectively at the left and right boundaries:

$$\begin{aligned} z_1^+ + z_1^- &= z_L^+ + z_L^-, \quad z_1^+ - z_1^- = (z_L^+ - z_L^-) \epsilon \\ z_3^+ + z_3^- &= z_R^+ + z_R^-, \quad z_3^+ - z_3^- = (z_R^+ - z_R^-) \epsilon, \end{aligned} \quad (7)$$

we use 1, L to denote the amplitudes at the position of the left T.R. (resp. 1 on the photospheric side, L on the coronal side), and 3, R to denote the amplitudes at the position of right T.R. (resp. R on the coronal side, 3 on the photospheric side); see [Fig. 2](#):

$$z_1^\pm = z^\pm(x=0^-) \quad (8)$$

$$z_L^\pm = z^\pm(x=0^+) \quad (9)$$

$$z_R^\pm = z^\pm(x=L_c^-) \quad (10)$$

$$z_3^\pm = z^\pm(x=L_c^+) \quad (11)$$

with the exponents $+$ or $-$ in 0 and L_c indicating whether we are on the right or the left side of the two T.R.s, located at $x=0$ and $x=L_c$, respectively.

To obtain the jump conditions to be effectively implemented in the three-layer model, we rewrite Eqs. (7) as follows. We denote by input what goes into the corona and output what goes

out. The coronal inputs z_L^+ and z_R^- are expressed in terms of the chromospheric inputs (z_1^+ and z_3^-) and the coronal outputs (z_L^- and z_R^+). Similarly the reflected chromospheric signals z_1^- and z_3^+ are expressed in terms of the chromospheric inputs and of the coronal outputs:

$$\begin{aligned} z_L^+ &= (1+a)z_1^+ - az_L^- \\ z_R^- &= (1+a)z_3^- - az_R^+ \\ z_1^- &= (1-a)z_L^- + az_1^+ \\ z_3^+ &= (1-a)z_R^+ + az_3^-. \end{aligned} \quad (12)$$

The parameter a

$$a = (1 - \epsilon)/(1 + \epsilon) \quad (13)$$

is the reflection coefficient. It is instructive to consider the limit $\epsilon = 0$. Then the coronal reflection coefficient a becomes unity. In this case, the velocity at the left coronal boundary is exactly z_1^+ ; that is, specifying the chromospheric input is the same as specifying the velocity (and the same at the right coronal boundary). This is the well-known line-tied limit. In this limit, the magnetic field fluctuation is not specified and depends on the coronal evolution, since one has $b_L/\sqrt{\rho} = -z_1^+ + z_L^-$. Returning to the general case with a nonzero Alfvén speed ratio ϵ , we see that specifying the chromospheric input does not directly determine the velocity at the T.R. either. We choose here to consider a nonzero input only from the left foot point (boundary), in order to follow the propagation of the incident signal better.

In the early work by [Hollweg \(1984\)](#), the three-layer model was studied analytically, with a damping term representing the effects of turbulence. As said, turbulent dissipation is highly intermittent thus requiring a description that goes beyond a simple damping term. We now define the nonlinear part of the model, i.e., the turbulence model.

The jump conditions just described are not specific of a linear framework. In the general case where the waves have a perpendicular structure and interact nonlinearly, the jump conditions hold as well. In the final model to be explained now, where the wave amplitudes depend on the coordinate along the loop and on an index n representing the perpendicular wavenumber k_n , the jump conditions are valid for each Fourier coefficient $z_n^\pm(x) = z^\pm(x, k_n)$ at $x=0$ and $x=L_c$, if 0 and L_c are the two coordinates of the transition region. In the following, the integer subscripts 1 and 3 will be used to label the layers as in [Fig. 2](#), while the Fourier modes will be labeled with the generic index n .

2.2. Nonlinear model: shell model for reduced MHD

In addition to the linear propagation of perturbations parallel to the loop mean field, we consider the waves to have a perpendicular structure, so that the wave-vectors also have nonvanishing components in planes perpendicular to the mean magnetic field. In this transverse direction nonlinear interactions between different perpendicular modes occur, while the dynamics of the parallel propagation (for a given perpendicular mode) remains purely linear. This model, known as reduced MHD or RMHD ([Strauss 1976](#)), is believed to be well adapted to situations with a large uniform axial field B_0 compared to perturbation amplitudes and strong anisotropy in the sense that the scales perpendicular to the field are shorter than the length of the coronal loop ([Rappazzo et al. 2007](#)):

$$\frac{\partial z_\perp^\pm}{\partial t} \mp \frac{B_0}{\sqrt{\rho}} \frac{\partial z_\perp^\pm}{\partial x} = -(z_\perp^\mp \cdot \nabla) z_\perp^\pm - \frac{1}{\rho} \nabla_\perp(p^T) + \nu \nabla_\perp^2 z_\perp^\pm, \quad (14)$$

where we have taken identical kinematic viscosity and resistivity, the density is uniform in the direction orthogonal to the field and the total pressure gradient guarantees the incompressibility of the z^\pm fields via the Poisson equation

$$\nabla_\perp^2(p^T) = -\nabla \cdot (z_\perp^\mp \cdot \nabla z_\perp^\pm). \quad (15)$$

A second approximation consists in transforming the perpendicular nonlinear couplings by replacing them, at each point on the x coordinate mesh along the mean field direction, by a dynamical system defined in Fourier space, which allows reaching a very high Reynolds number compared to genuine reduced MHD. This is known as the shell model for RMHD or hybrid shell model (Nigro et al. 2005; Buchlin & Velli 2007). The Reynolds number gain can be quantified as follows. Assume K is the perpendicular resolution (ratio from largest to smallest scales). Assume also the parallel resolution scales as $K^{2/3}$. When passing from the RMHD to shell RMHD, the number of degrees of freedom changes from $K^{2+2/3}$ to $K^{2/3} \text{Log}_2(K) \simeq K^{2/3}$ (see below). The CPU time required to describe the same large-scale evolution is proportional to this number multiplied by K . Conversely, the reachable resolution goes as the CPU time T as $T^{3/11}$ in the RMHD case and as $T^{3/5}$ in the shell RMHD case, thus passing from a resolution K_0 to a resolution $K_0^{11/5}$. The same is true for the Reynolds number (which goes as a power of the resolution K), hence typically passing from 10^3 to 10^6 .

Coronal heating driven by photospheric motions has been studied using both RMHD and RMHD shell models in a one-layer atmosphere (corona) version, with uniform Alfvén speed and closed (line-tied) boundaries, i.e. imposing the photospheric perpendicular velocity at loop foot points. Here we use an RMHD-shell model, but in the three-layer context, that is, including the linear jump laws defined previously at the transition region for each of the perpendicular wave numbers.

The shell model is characterized by the number $N + 1$ of perpendicular wave modes, each characterized by a perpendicular wave number, with amplitudes z_n^\pm (the direction of the wave vector is not specified in the model), with the following discretization:

$$k_n = 2^n k_0 \quad n = 0 \dots N. \quad (16)$$

Starting from the RMHD equations, one can write the following simplified equations (see Buchlin & Velli 2007, for the full equations with inhomogeneous density):

$$\begin{aligned} \partial_t z_n^+ + V_a \partial_x z_n^+ &= T_n^+ - \nu k_n^2 z_n^+ \\ \partial_t z_n^- - V_a \partial_x z_n^- &= T_n^- - \nu k_n^2 z_n^- \end{aligned} \quad (17)$$

where V_a is either V_a^0 (chromosphere) or V_a^c (corona), ν is the kinematic viscosity (equal to the magnetic diffusivity), and the T_n^\pm are the nonlinear terms that are a sum of terms of the form $T_n^\pm = A k_m z_p^\mp z_q^\pm$ with m , p , and q close to n (see Biskamp 1994; Giuliani & Carbone 1998, for the full expression of T_n^\pm).

From the basic Eqs. (17), one can deduce the (exact) energy budget equation of a flux tube of length L , section $\pi l_{\perp 0}^2$, and density ρ (assumed constant) as

$$dE/dt = F(t) - D(t). \quad (18)$$

Here E is the total energy, F the energy flux, and D the energy dissipation rate defined as

$$\begin{aligned} E &= M \frac{1}{2L} \int_0^L dx (u^2 + b^2/\rho) \\ &= M \frac{1}{4L} \int_0^L dx [(z^+)^2 + (z^-)^2] \end{aligned} \quad (19)$$

$$F = M V_a \frac{1}{4L} [(z_0^+)^2 - (z_L^+)^2 + (z_L^-)^2 - (z_0^-)^2] \quad (20)$$

$$D = M \frac{1}{2L} \int_0^L dx \sum_{n=0}^N \nu k_n^2 (z_n^{+2} + z_n^{-2}). \quad (21)$$

Here, $M = \pi l_{\perp 0}^2 L \rho$ is the mass of the loop system, u^2 and b^2/ρ , $(z^+)^2$, $(z^-)^2$ are the sum of the energies per unit mass in all the modes $n = 0 \dots N$. When applying Eq. (18) to the corona, we take $\rho_c = \epsilon^2 \rho_0$, $V_a = V_a^c$, and the subscripts (integration interval) 0, L represent the left and right coronal boundaries, respectively (not including the chromosphere when it is present). The parameter $l_{\perp 0}$ stands for the largest scale available in the simulation, which in all runs is always $l_{\perp 0} = 4l_\perp$. In the following, we use the notations E, D, F as defined in Eqs. (19)–(21) but always normalized by the total mass M of the loop system, so obtaining average energies and dissipation rates per unit mass.

Several remarks are in order. First, the nonlinear terms do not appear in the energy budget Eq. (18), because the total energy is conserved by nonlinear coupling, as much in the reduced MHD equations as in the presently used shell model version of the equations. Second, the energy accumulated or lost by the corona is not directly controlled. Indeed, the energy flux entering the corona (Eq. (20), see also the more explicit Eq. (25) below) is determined by the difference between the incoming and outgoing energies at the two transition regions; as is made clear in the next section, the boundary conditions fix the incoming amplitudes, possibly in terms of the outgoing amplitudes, but not the energies.

2.3. Boundary and jump conditions for three- and one-layer model

As a rule, boundary conditions are defined by imposing the value of z_n^+ at $x = 0$ (the rightward propagating wave amplitude) and the value of z_n^- at the boundary $x = L$ (the leftward wave amplitude).

2.3.1. Closed model (line-tied)

The loop only contains the corona. The usual closed or line-tied model has

$$\begin{aligned} z_n^+(x = 0, t) &= 2U_n^0(t) - z_n^-(x = 0, t) \\ z_n^-(x = L, t) &= 2U_n^L(t) - z_n^+(x = L, t) \end{aligned} \quad (22)$$

for boundary conditions. This equation results from Eqs. (12) with $a = 1$, $z_L^+ \equiv z_n^+(x = 0, t)$, and $z_R^- \equiv z_n^-(x = L, t)$. The z_L^+ (z_R^-) signal in the corona is obtained by prescribing the *velocity amplitude* U_n^0 (U_n^L) of each mode n at the boundary $x = 0$ ($x = L$). One checks from Eq. (22) that, when $U_n^{0,L} = 0$, then the energy flux (Eq. (20)) injected in the domain indeed becomes zero.

2.3.2. One-layer model

In this first model including leakage, the chromosphere is excluded from the domain, the domain boundaries coinciding with

the T.R., as in the closed model. The boundary conditions now take the wave jump conditions ($a < 1$ in Eqs. (12)) explicitly into account:

$$\begin{aligned} z_n^+(x=0, t) &= (1+a)Z_n^+(t) - az_n^-(x=0, t) \\ z_n^-(x=L, t) &= (1+a)Z_n^-(t) - az_n^+(x=L, t). \end{aligned} \quad (23)$$

The quantities Z_n^+ and Z_n^- now denote the prescribed *wave amplitudes* entering from the chromospheric side of the transition region. With reference to Fig. 2 we have $Z_n^+ \equiv z_1^+$ and $Z_n^- \equiv z_3^-$.

2.3.3. Three-layer model

In this second model allowing leakage, the chromosphere is really included within the domain; in that case, the boundary conditions (at the photosphere) are chosen to be purely open ($a = 0$ in Eqs. (12) or equivalently in Eq. (23)):

$$\begin{aligned} z_n^+(x=0, t) &= Z_n^+(t) \\ z_n^-(x=L, t) &= Z_n^-(t). \end{aligned} \quad (24)$$

The boundaries are open in the sense that incoming waves are defined independently of outgoing waves, which in turn generate no incoming wave, so that they escape freely from the domain: perturbations coming from the loop reach the boundary and disappear below the boundary without reflection. Wave reflections and transmissions continuously occur within the domain at the location of the transition regions, where we apply the jump conditions (Eqs. (12)), for each perpendicular mode n .

The three-layer model and the one-layer model with partially reflecting boundaries are parametrized by the same number ϵ , the photospheric/coronal Alfvén speed ratio. The two models thus both include the transmission and reflection of waves by the transition region, but have an important difference. In the one-layer model, the chromospheric input is specified, as the T.R. coincides with the boundary of the domain. Instead, in the three-layer model, the chromospheric input (z_1^+ , z_3^- in Fig. 2) is not prescribed, since the (prescribed) photospheric input has been modified by turbulence during its propagation through the chromosphere. Both models have specific advantages: the three-layer model has more internal degrees of freedom, as it shows two distinct (but coupled) turbulent layers, one in the chromosphere, the other one in the corona. On the other hand, the one-layer model is more directly comparable to the closed line-tied model: the domain is the same (the corona), only the boundary conditions change. We study both models, with some emphasis on the three-layer model.

In the simulations we present, forcing is applied by injecting upward propagating waves only at the left loop foot point; more precisely, the leftward propagating amplitude at the right photospheric foot point $Z_n^-(t)$ will be maintained zero in Eqs. (23), (24). In the particular case of the closed model (Eq. (22)), this means that the velocity at the right foot point $U_n^L(t)$ was kept zero. In this case, it is interesting to write down the expression for the net coronal energy flux:

$$\begin{aligned} F \propto \sum_n \Big\{ (1+a)^2 |z_1^+|^2 - 2a(1+a) \text{Re}(z_1^+ \cdot z_L^{\star}) \\ - (1-a^2) |z_L^-|^2 - (1-a^2) |z_R^+|^2 \Big\}. \end{aligned} \quad (25)$$

In the previous formula, the \star denotes the complex conjugate, indices n are assumed for each variable, and we have used the notations of Fig. 2, so the formula applies to the three models. We consider in turn the different terms on the righthand side.

The last two terms are always negative: they thus represent a pure leakage (and they indeed vanish for $a = 1$, in the closed or line-tied model). The first term is always positive and represents the continuous energy injection. The second term is fluctuating and is the only term that can cause leakage in the closed model. In the closed case, however, it is non zero only for the injected modes (which are at large scales, see next section), due to the presence of the z_1^+ factor, which strongly limits the leakage in the closed case.

2.4. Parameters and timescales

The parameters of the model are the length of the chromospheric and coronal parts of the loop L_{ch} , L_c respectively; the photospheric-chromospheric Alfvén speed, V_A^0 ; the Alfvén speed contrast ϵ ; the width of the loop $l_{\perp 0}$; the turbulent correlation scale l_{\perp} ; and the amplitude of the forcing at the left photosphere, U_0 . In all the models we always force by injecting an Alfvén wave: U_0 is the wave amplitude which is generally not directly related to the photospheric velocity shear. Only in the closed model do the two quantities coincide (see Sect. 2.1). The input photospheric spectrum is distributed on the perpendicular scales l_{\perp} , $l_{\perp}/2$, $l_{\perp}/4$, and will have a correlation time given by T_f , which completes the set of parameters.

For all the simulations we set $V_A^0 = 700$ m/s, $L_{\text{ch}} = 2$ Mm (so that L scales with L_c only); i.e., we assume that photospheric values are independent of the loop length and that all loops have a transition region. We also set $l_{\perp} = l_{\perp 0}/4$ and $T_f = \infty$. The rest of the parameters l_{\perp} , L_c , U_0 , ϵ define the following physical timescales (i.e., input of the model): the leakage time, the coronal Alfvén time, and the input nonlinear time (which rules the strength of the turbulence resulting from the driving):

$$t_L = L_c/V_A^0 \quad (26)$$

$$t_a^c = L_c/V_A^c = \epsilon t_L \quad (27)$$

$$t_{NL}^0 = l_{\perp}/(2\pi U_0). \quad (28)$$

We also fix $L_c = 6$ Mm and $\epsilon \approx 0.02$, thus only t_{NL}^0 will be varied at fixed t_a^c and t_L , by changing the parameters U_0 and l_{\perp} . In a subsequent paper we will study the effects of varying the leakage and the Alfvén timescales. From these characteristic times we define the following dimensionless parameters that measure the nonlinear term vs. the two main linear effects (the Alfvén wave propagation and the leakage):

$$\chi_L = t_L/t_{NL}^0 \quad (29)$$

$$\chi_0 = t_a^c/t_{NL}^0 = \epsilon \chi_L. \quad (30)$$

The parameter χ_0 has been used by [Dmitruk et al. \(2003\)](#), [Rappazzo et al. \(2008\)](#), and [Nigro et al. \(2008\)](#) to quantify the turbulent behavior in their studies of turbulence forcing with closed boundaries (corresponding to $\chi_L = \infty$).

Figure 3 shows the plane with χ_0 in abscissa and χ_L in ordinate. This plane is divided in four quadrants by the lines $\chi_0 = 1$ and $\chi_L = 1$. There are actually only three subsets left, as only the subset with $\epsilon < 1$, visible as the unshaded region of Fig. 3, is permitted, due to the stratification. Turbulence is said to be weak (in the left part) or strong (right part), depending on χ_0 being smaller or larger than unity. In the two upper quadrants, which occupy most of the domain, leakage should be negligible. Only in the small (left) bottom region should leakage dominate turbulent loss.

The two curves represent each a family of coronal loops of varying length L , build from a two-temperature hydrostatic

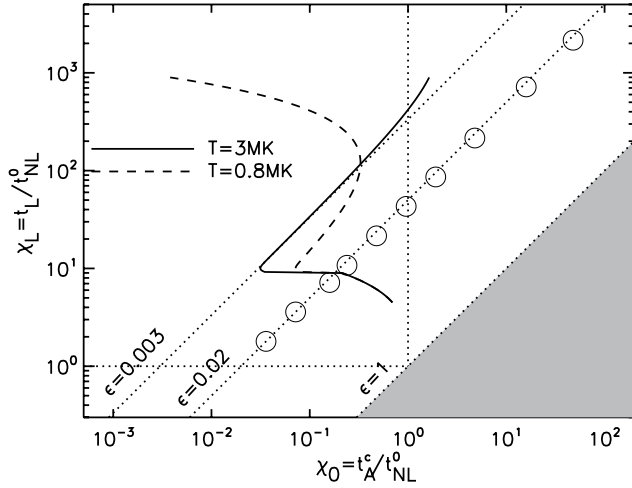


Fig. 3. Characteristics of typical solar loops compared with simulation parameters: χ_L versus χ_0 . The turnover time is fixed to $t_{NL}^0 = 1000$ s and we assume a two-temperature hydrostatic loop model (see appendix). The black solid and dashed lines are for the two coronal temperatures of 3 MK and 0.8 MK, respectively. The circles are for the three-layer runs A–L (see Table 1). The diagonal dotted lines are the curve $\chi_L = (1/\epsilon)\chi_0$ for three values of ϵ .

model (see Appendix A), which leads to a function $V_a^c(L)$. The loop length L increases from bottom to top (i.e., with increasing χ_L) from 3 to 700 Mm. Most of the hot loops show an Alfvén speed contrast of $\epsilon = 0.003$, about ten times lower than the ϵ value chosen for the three-layer simulations. The choice of relatively high ϵ values for the simulations comes from the requirement of having a reasonable value for the ratio of integration time to single time step.

We now give a brief account of the physical and numerical timescales. Taking for instance $l_\perp = 2$ Mm, with $N = 20$ perpendicular wave modes, the highest available perpendicular wavenumber will be $k_{\max} = 1.600$ 1/km. The shortest nonlinear time (evaluated at the maximum perpendicular wavenumber in the corona) will be, if z_c is the typical coronal amplitude (z denoting either z^+ or z^-),

$$\tau_{NL} = 1/(k_{\max} z_c) \simeq \epsilon/(k_{\max} U_0) \quad (31)$$

where we have taken the resonant linear case (see next section) for which the wave amplitudes are larger by a factor $1/\epsilon$ in the corona. Replacing by previous values and assuming $\epsilon = 0.01$, we obtain for the smallest nonlinear time

$$\tau_{NL} \simeq 6 \times 10^{-5} \text{ s}. \quad (32)$$

As a matter of comparison, we use $N_\parallel = 10^4$ grid points to describe space along the loop, so that, for a typical loop length $L = 6$ Mm, we obtain

$$\tau_\parallel = 1/(k_\parallel^{\max} V_a^c) = \epsilon L/(\pi N_\parallel V_a^0) \simeq 2 \times 10^{-3} \text{ s} \quad (33)$$

for the shortest linear time for parallel propagation in the corona. As a result, the constraint on the time step comes from the perpendicular nonlinear time. Finally, at least in the linear case (see next section), the characteristic time for large-scale evolution is the long leakage time:

$$t_L = L/(V_a^0) \simeq 9 \times 10^3 \text{ s}. \quad (34)$$

Comparing Eqs. (32)–(34), we see that $\approx 10^8$ time steps of a dynamical system with $2 \times 20 \times 10^4$ degrees of freedom are necessary to achieve one (anticipated) characteristic evolution time of the system.

Table 1. Parameters for the the simulations.

Run	ϵ (adim)	L_c (Mm)	l_\perp (Mm)	U_0 (km s ⁻¹)	χ_0 (adim)	χ_L (adim)
A	0.020	6	1.500	0.05	0.04	1.8
B	0.020	6	1.500	0.10	0.07	3.6
C	0.022	6	1.500	0.20	0.16	7.2
D	0.022	6	0.500	0.10	0.24	11
E	0.022	6	0.500	0.20	0.48	22
F	0.022	6	0.250	0.20	0.96	43
G	0.022	6	0.125	0.20	1.9	86
H	0.022	6	0.025	0.10	4.8	215
I	0.022	6	0.008	0.10	16	718
L	0.022	6	0.003	0.10	48	2154
A _{IL}	0.020	6	1.500	0.025	0.02	0.9
B _{IL}	0.020	6	1.500	0.10	0.07	3.6
C _{IL}	0.020	6	1.500	0.20	0.14	7.2
D _{IL}	0.020	6	0.500	0.10	0.22	11
E _{IL}	0.020	6	0.125	0.10	0.86	43
F _{IL}	0.020	6	0.063	0.10	1.7	86
G _{IL}	0.020	6	0.025	0.10	4.3	215
H _{IL}	0.020	6	0.008	0.10	14	718
I _{IL}	0.020	6	0.003	0.10	43	2154
A _{cl}	0	6	1.500	0.025	0.02	∞
B _{cl}	0	6	1.500	0.10	0.07	∞
D _{cl}	0	6	0.500	0.10	0.22	∞
E _{cl}	0	6	0.125	0.10	0.86	∞
F _{cl}	0	6	0.063	0.10	1.7	∞
G _{cl}	0	6	0.013	0.10	8.6	∞
H _{cl}	0	6	0.003	0.10	43	∞

Notes. The three subpanels refer to the three-layer, one-layer, and closed models in which boundary conditions are open (three-layer), half reflecting (one-layer), and line-tied (close). For all runs, $T_i = \infty$, $V_a^0 = 0.7$ km s⁻¹, $L_{ch} = 2$ Mm (except for runs H, I, L that have $L_{ch} = 1$ Mm). ϵ denotes the ratio of photospheric over coronal Alfvén speed (plays no explicit role in the closed model). L_c is the length of the coronal part of the loop. l_\perp is the perpendicular largest injection scale (the injected energy is distributed on scales l_\perp , $l_\perp/2$, and $l_\perp/4$). U_0 is the amplitude of the input wave. χ_0 is the linear to nonlinear time ratio (Eq. (30)), χ_L is the leakage to nonlinear time ratio (Eq. (29)).

3. Phenomenology

3.1. Linear coronal trapping and leakage

We first recall the linear result in the zero-frequency case, i.e. when forcing is time independent; a transverse perturbation (here, any perpendicular mode) is subjected to successive transmission-reflection at the two coronal bases, left and right. Since nonlinear interactions are ignored, all modes show the same evolution. As shown in Grappin et al. (2008) for a loop with smooth variation in the Alfvén speed, the level of z^+ and z^- grows progressively in the corona, in such a way as to achieve the asymptotic values

$$z^+ \simeq -z^- \simeq b/\sqrt{\rho} = U_0/\epsilon \quad (35)$$

over a long timescale t_L . In other words, the asymptotic solutions are a uniform magnetic field amplitude everywhere along the loop at equipartition with the photospheric energy density, as well as a uniform velocity fluctuation everywhere along the loop. The asymptotic state is thus the same as would be achieved if the plasma were completely transparent to Alfvén waves ($\epsilon = 1$):

$$u = U_0, \quad b = b_0 = B_0 U_0 / V_a^0, \quad (36)$$

although this happens on the long timescale $t_L = L/V_a^0$ and not on the short Alfvén coronal time t_a^c (we assimilate here and

in the following the coronal length to the total loop length L). Typically, if the shear amplitude is $U_0 = 0.1$ m/s and the mean field $B_0 = 100$ G, then the equilibrium magnetic field associated with the shear is the equipartition field, that is, $b_0 \simeq 14.5$ G.

3.2. Resonant response

Consider the simplest case where the frequency of the photospheric input is either zero or resonant (that is, equal to n/t_a^c , with n an integer ≥ 0). The coronal field perturbation induced by the photospheric field perturbation $U_0 = b_0/\sqrt{\rho_0}$ grows linearly with time until it saturates at a finite value because of the two damping losses, the linear leakage (with timescale t_L) and the nonlinear turbulent damping (with timescale t_D):

$$\partial_t b = B_0 U_0 / L - b/t_L - b/t_D = B_0 U_0 / L - b/t_\eta \quad (37)$$

$$= b_0/t_L - b/t_\eta \quad (38)$$

where $b_0 = 14.5$ G is the photospheric magnetic perturbation, and t_η is the effective damping time:

$$t_\eta = (1/t_L + 1/t_D)^{-1}. \quad (39)$$

In Eq. (38) we have rewritten the first term using the definition $t_L = L/V_a^0$ in order to illustrate the fact that, in the absence of dissipation ($t_D = \infty$, $t_\eta = t_L$), the trapping and leakage times are equal.

The stationary solution is for the coronal field perturbation:

$$b = U_0 (t_\eta B_0 / L) \quad (40)$$

$$= b_0 / (1 + t_L/t_D). \quad (41)$$

One sees that the coronal response is maximal (equal to the photospheric value $b_0 = 14.5$ G) when no turbulent damping is present ($t_D \gg t_L$). In the other limit ($t_L \gg t_D$), turbulent damping limits the coronal field to a fraction b_0 : $b \simeq b_0 t_D / t_L = t_D B_0 U_0 / L$.

Relation (41) may be rephrased in terms of energy per unit mass as

$$E = E_0 (t_\eta / t_a^c)^2 \quad (42)$$

with $E_0 = 1/2(U_0^2 + b_0^2/4\pi\rho_0) = U_0^2$. In the case where $t_D \ll t_L$, Eqs. (41)–(42) have already been given by [Hollweg \(1984\)](#); as pointed out by [Nigro et al. \(2008\)](#), they are also valid for the zero-frequency case (see also [Grappin et al. 2008](#)), the only difference being that in the latter case magnetic energy is dominant in the corona, while in the case of nonzero resonance coronal magnetic and kinetic energies are at equipartition.

A last remark concerns the use of Eqs. (38) and (41) (but not Eq. (42)). Caution must be taken when applying the lined-tied limit, $t_L = \infty$, since the trapping time, appearing as t_L in these equations, is finite and fixed. The explicit forms, Eqs. (37) and (40), are therefore better suited to understanding the difference between the opened and closed models. In particular, one sees that the coronal magnetic field grows linearly with time in the absence of dissipation (Eq. (37)) while, when dissipation is present, it can grow well beyond the leakage-limited value b_0 (Eq. (40)), since the loss timescale t_η has no upper limit².

² As we see in the closed model the dissipation timescale can be larger than the nominal value t_L (see Fig. 13), thus leading to $b > b_0$.

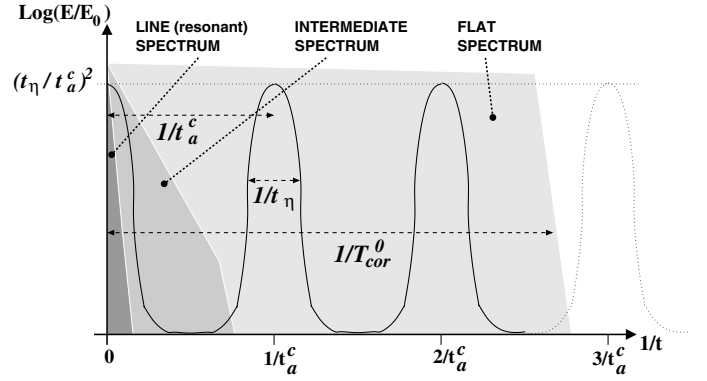


Fig. 4. Sketch of the linear coronal energy gain, $\log(E/E_0)$ as a function of frequency. E_0 is the input photospheric energy at each frequency. It is assumed that $t_a^c \ll t_\eta$, and only the non-wkb portion of the spectrum is shown. The injected spectrum is also indicated as a shaded areas on an arbitrary scale, for the case of flat, intermediate, and line spectra (in increasing gray-scale order).

3.3. The general case

In general, the signal injected into the corona is not necessarily resonant and more generally not monochromatic. To quantify both the trapped energy and its dissipation rate we need to know how the time-dependent energy input is distributed between resonant and nonresonant frequencies. We thus introduce the correlation time of the energy T_{cor}^0 entering the corona or equivalently the width of the injection spectrum $1/T_{\text{cor}}^0$, which is a priori unknown.

Recalling that the resonant lines are spaced each $1/t_a^c$, each with a width equal to the inverse of the damping time t_η , then we may distinguish several cases depending on the portion of the excited spectrum (see Fig. 4):

- Flat spectrum: $T_{\text{cor}}^0 < t_a^c$. Negligible energy being transmitted outside the resonant lines (enlarged by damping) compared to the energy transmitted for frequencies within the lines (anti-resonances) leads to a filling factor equal to t_a^c/t_η compared to a spectrum made of only resonant frequencies (Eq. (42)).
- Intermediate T_{cor}^0 : $t_a^c < T_{\text{cor}}^0 < t_\eta$. Then the filling factor is T_{cor}^0/t_η as only the zero-frequency resonance and the first anti-resonance are excited.
- Long correlation time or resonant spectrum: $t_\eta < T_{\text{cor}}^0$. This coincides with the linear resonant gain Eq. (36) if $t_L \ll t_D$.

Finally,

$$E = E_0 (t_\eta / t_a^c) \quad (T_{\text{cor}}^0 < t_a^c) \quad (43)$$

$$E = E_0 (t_\eta / t_a^c) T_{\text{cor}}^0 / t_a^c \quad (t_a^c < T_{\text{cor}}^0 < t_\eta) \quad (44)$$

$$E = E_0 (t_\eta / t_a^c)^2 \quad (t_\eta < T_{\text{cor}}^0). \quad (45)$$

We transformed Eq. (44), which originally reads as $E = E_0 (t_\eta / t_a^c)^2 T_{\text{cor}}^0 / t_\eta$. Equations (43), (44) have been derived for negligible leakage ($t_\eta = t_D$), in the strong turbulence case by [Hollweg \(1984\)](#) and in the weak turbulent case by [Nigro et al. \(2008\)](#). The relations proposed here extend these early findings by including the case where leakage dominates turbulence and the case of very weak turbulence (resonant spectrum).

To make these expressions explicit, one should express the unknown parameters in terms of control parameters. It is tempting for instance to identify T_{cor}^0 with t_{NL}^0 : then the three regimes correspond respectively to strong turbulence ($\chi_0 > 1$), weak turbulence ($\chi_0 < 1$), and weak dissipation ($\chi_L < 1$).

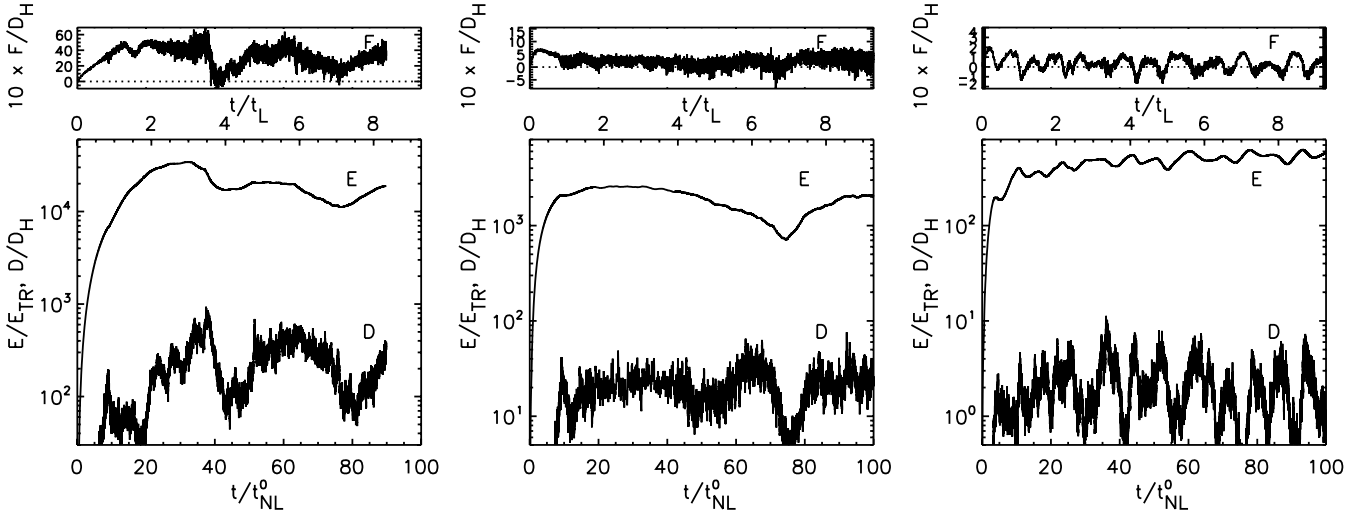


Fig. 5. From left to right: Run D_{cl} (closed model), Run D_{IL} (one-layer model), and Run D (three-layer model). For all the runs $\chi_0 \approx 0.2$, for the one-layer and three-layer models $\chi_L \approx 11$. *Top panels:* time evolution of the net energy flux F . *Bottom panels:* time evolution of the coronal energy (E) and dissipation below (D). Time is normalized to the input nonlinear timescale t_{NL}^0 , energy is normalized to the injection energy at the left boundary $E_{TR} = U_0^2$, dissipation and flux are normalized to Hollweg expression $D_H = E_{TR}/t_a^c$.

Indeed, the last condition ($\chi_L < 1$) can only be satisfied if $t_L < t_D$ since we exclude the possibility that $t_D < t_{NL}^0$. Thus assuming $T_{cor}^0 = t_{NL}^0$, the line spectrum coincides with the linear resonant gain and can only be reached by imposing $\chi_L < 1$. If the injection spectrum has a finite width, a possible choice is $T_{cor}^0 = \min(T_f, t_{NL}^0)$ as suggested by Malara et al. (2010). If $T_f > t_{NL}^0$, we fall into the previous case. If instead $T_f < t_{NL}^0$, the ordering considered in Nigro et al. (2008) and Malara et al. (2010), the line spectrum is not achievable. However, as we will see, the correlation time may also be given by other timescales, such as the leakage time t_L or the chromospheric crossing time $t_a^{ch} = L_{ch}/V_a^0$. The remaining (difficult) task is to express the dissipation time t_D (since $t_\eta = \min(t_D, t_L)$), in terms of χ_0 and χ_L via the coronal nonlinear time. We will come back to this point later on.

3.4. Dissipation in the strong and weak regimes

In the strong turbulence case ($\chi_0 > 1$), dissipation is expected to dominate leakage, and a simple explicit expression of the dissipation rate is obtained after replacing $t_\eta = t_D$ in Eq. (43) (Hollweg 1984):

$$D = E/t_D = E_0/t_a^c. \quad (46)$$

This relation is attractive, because it leads to a universal result: the heating rate per unit mass does not depend on the detail of turbulent dissipation, since it only depends on the length of the loop and the photospheric energy. However, this universality is lost when we turn to the weak turbulent regime, $\chi_0 < 1$, Eq. (44), which we have seen is probably prevalent in the corona (Fig. 3). To extrapolate the previous expression (Eq. (46)) to the weak regime with $\chi_0 < 1$, we identify T_{cor}^0 with t_{NL}^0 in Eq. (44) and still adopt $t_D < t_L$:

$$D = E/t_D = E_0/t_a^c (1/\chi_0). \quad (47)$$

This predicts that the weaker the turbulence regime, the higher the dissipation. We will see that both relations (46), (47) are reasonably satisfied if we use the line-tied limit, but not in the more

realistic open case. In the open case, we find that Hollweg's expression (Eq. (46)) actually holds more or less both for $\chi_0 > 1$ and $\chi_0 < 1$, which requires admitting that $t_D > t_L$ in the weak regime, i.e., that the dissipation time becomes very long as turbulence weakens.

4. Results

In the following we compare first the different models in a weak turbulence case, the most probable for coronal conditions. Then we focus on the three-layer model and compare the weak and strong turbulence regimes.

4.1. How leakage changes turbulence: the weak turbulence case

We consider here a weak turbulent case with $\chi_0 \approx 0.2$, and compare the closed, one-layer, and three-layer models. The runs are D_{cl}, D_{IL}, and D respectively in Table 1; in the open models $\chi_L \approx 11$ so we expect that turbulence is the main channel for energy loss in all models. Because of this, we should not expect significant differences between the closed and the one-layer run. However, we might perhaps find differences due to the different forcing (from now on we will use forcing to mean injection into the corona) between the one-layer and the three-layer runs, recalling that forcing is constant in the first case, and time-dependent in the second, due to the possibility of a chromospheric turbulence.

The time evolution of the corona in the three models (from left to right) is summarized in Fig. 5 where the entering energy flux F (top panel), the total energy E , and dissipation D (bottom panel) are shown (see Eqs. (19)–(21)). Time is normalized to the input nonlinear timescale, t_{NL}^0 ; energy is normalized to the input coronal energy $E_{TR} \equiv z_{TR}^2/4$; and the dissipation and the flux are normalized with respect to Hollweg expression, $D_H \equiv E_{TR}/t_a^c$ (for the closed and one-layer model $z_{TR} \equiv U_0$; for the three-layer model, z_{TR} is the measured quantity z_1^+ that is not directly controlled by the boundary conditions).

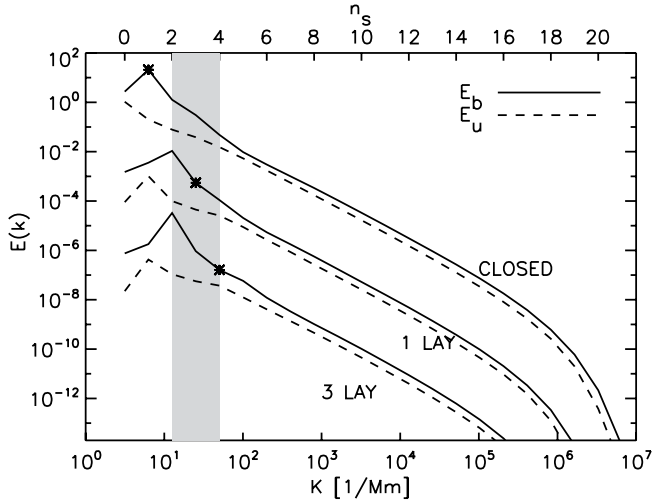


Fig. 6. Coronal kinetic energy spectrum (dashed line) and magnetic energy spectrum (solid line) for runs D_{cl} , D_{1L} , and D . Wavenumbers are in units of $1/\text{Mm}$ and in the top x -axis the corresponding shell numbers are indicated. The spectra are averaged in time and space and the normalization is in arbitrary units (spectra are also rescaled). The symbols on the E_b spectra indicate the first shell number for which $t_{NL}^u(k) = 1/ku(k) < t_a^c$.

A quick look at the energy flux curves shows a sharp contrast between the closed run and the open one-layer run. While in the closed case, the coronal energy flux is almost always positive, but in the open case, it is constantly oscillating around zero, although with a positive mean value flux. This has an immediate corollary: the energy level shows much lower values in the open case. Another corollary is that the dissipation rate itself, i.e., coronal heating, is reduced by a factor ten. This tendency is sharply enhanced in the case of the three-layer model, which shows a further reduction of a factor 5. Another remarkable difference appears in the three-layer model, which accounts for the chromospheric turbulence. The energy and the energy flux display quasi-periodic oscillations that are absent in the closed and one-layer models whose energy time series are shaped by the time-independent forcing. Such oscillations have a periodicity of about one leakage time or less (see the top horizontal axis in the bottom panel). However, we cannot rule out that their origin lies in the chromospheric turbulence. Indeed, the periodicity happens to be close to two chromospheric crossing times $2t_a^{\text{ch}} = 2L_{\text{ch}}/L_c t_L = 2/3 t_L$, which we interpret as the timescale needed for waves injected from the left footpoint to leave the chromospheric layer (a round trip of the chromosphere). Most probably such oscillations come from the coupling of the chromospheric and coronal turbulence and both timescales matters, as we see in Sect. 4.3.

Figure 6 shows the time and space-averaged kinetic and magnetic spectra in the corona for the three models. One sees that all cases show well-developed power-law ranges, plus a magnetic hump at large scales. The (common) forcing range is represented by a gray vertical band and the symbol on the magnetic spectrum marks the largest scale for which the effective nonlinear time computed on the rms velocity at that scale is shorter than the Alfvén crossing time. The only significant difference visible between the three spectra is that the magnetic peak is located at the largest forcing scale for the open runs, while it has migrated to a scale that is larger by a factor two for the closed run. This indicates that an inverse transfer is active in all cases, but that it is more active in the closed case, or also possibly that

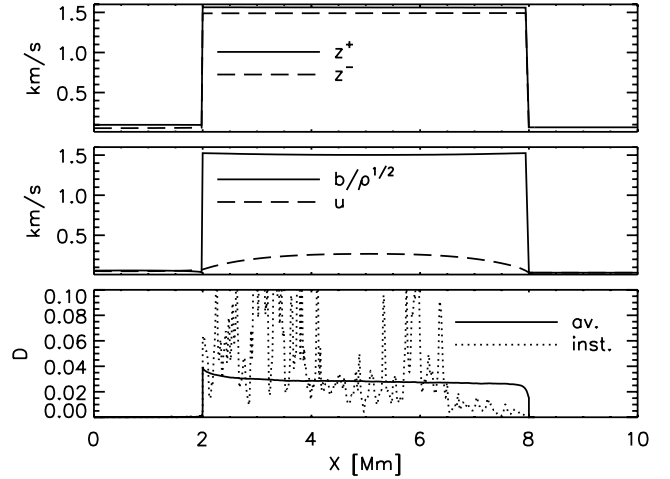


Fig. 7. Run D (three-layer open model, weak turbulence case): spatial distributions of fluctuations (*top and mid panels*) and turbulent heating (*bottom panel*). The time-averaged rms amplitude (in km s^{-1}) are plotted as a function of loop coordinate (in Mm) for z^+ , z^- (*top panel*, solid and dashed lines, respectively) and for $b/\sqrt{4\pi\rho}$, u (*bottom panel*, solid and dashed lines, respectively). The time-averaged heating rate (in arbitrary units) is plotted in the *bottom panel* as a solid line, and a snapshot is shown in dotted line.

it has been hindered by leakage of the largest scales in the open cases.

We are thus forced to conclude that, in the open models, despite the fact that $\chi_L > 1$, the energy accumulation is limited by leakage. This means that the nonlinear timescale t_{NL}^0 is a sharp under-estimation of the real dissipation timescale. We come back on this point in the following.

4.2. The three-layer model: chromosphere vs corona

We describe here the structure of the open three-layer model in the weak turbulence case. In particular we compare the chromosphere and corona. We show in Fig. 7 the spatial profiles in the corona and chromosphere of the fluctuations and of the dissipation rate. The top panel shows the time average of the rms value z^+ and z^- amplitudes with z_{rms}^{\pm} defined as

$$z_{\text{rms}}^{\pm} = \sqrt{\sum_n |z_n^{\pm}|^2}. \quad (48)$$

The mid panel shows the time-averaged rms values of velocity u and magnetic field in km s^{-1} units ($b/\sqrt{\rho}$). The bottom panel shows the time average and a snapshot of the heating rate.

In spite of the presence of turbulence (as revealed by the spectra examined above), the rms amplitudes of all quantities are seen to be remarkably smooth functions of loop coordinates except of course at the T.R. Main features are (1) that the magnetic field amplitude in the corona and chromosphere are actually comparable (the magnetic field amplitude plotted in the figure is $b/\sqrt{4\pi\rho}$, hence a factor of about $1/\epsilon = 50$ between the coronal and chromospheric values); (2) that the velocity contrast is significantly greater than unity but much smaller than the magnetic contrast (in units of velocity), and its coronal profile has a simple form; and (3) that the z^+ and z^- levels are comparable in the corona.

Feature (1) implies that the main part of the magnetic energy trapped in the corona is actually close to the linear state of zero

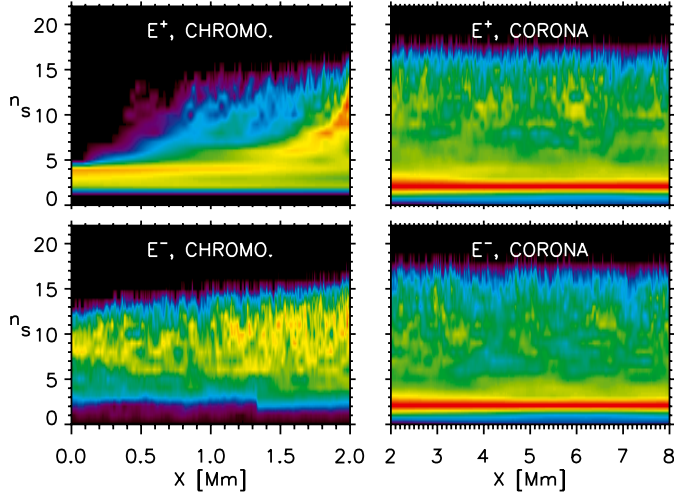


Fig. 8. Run D. Contour plot of the spectra $E^\pm(x, k_n)$ (snapshots) for z^+ and z^- (top and bottom panels, respectively) compensated for $k^{5/3}$ in the chromosphere (left panels) and in the corona (right panels). Ordinate: shell number $n_s = \log_2(k_n/k_0)$. Abscissa: coordinate x along the loop in Mm. The contours have different ranges in the chromospheric and coronal layers to highlight their structures better.

resonance (in the linear case with zero frequency the asymptotic coronal magnetic field fluctuations is equal to the photospheric field, see Grappin et al. 2008). (2) The coronal profile of the velocity field is actually close to the profile of the first linear resonance (Nigro et al. 2008). Feature (3) allows full nonlinear coupling that is compatible with the existence of a developed spectrum.

Nigro et al. (2008) have already found in the closed case that the characteristic linear resonance profiles of the coronal cavity are not deeply affected by the presence of a nonlinear cascade. It appears that the same linear resonance profiles are not affected by leakage either.

Finally, the time-averaged profile of the average dissipation rate per unit mass (bottom panel in Fig. 7) shows that the chromospheric dissipation remains negligible, and also that the left T.R. (i.e. above the foot point where energy is injected) is dissipating at a slightly higher rate than the other foot point. A typical snapshot is also shown, providing a hint of the substantial intermittency of the heating rate, both in space and time.

The turbulent activity of both the chromosphere and corona are shown in Fig. 8, in which we plot snapshots of the z^- and z^+ spectra $E^\pm(x, k_\perp)$ (top and bottom panels) respectively in the left chromosphere and corona (left and right panels). The spectra are compensated for $k^{5/3}$ in both layers. The motivation for plotting z^\pm spectra instead of u and b spectra is to make the respective contributions of the chromosphere and corona to the spectral formation clear, since the directions of propagation are identifiable for z^\pm , not for u and b . Only the left chromosphere has been represented (since the evolution is purely linear in the right chromosphere, due to the absence of z^- input from the right foot point), its length has been enlarged to make its structure more conspicuous, and the contours have different ranges in the chromosphere and in the corona.

One can see in the figure something like the trajectory of turbulence from the left foot point to the corona and all the way back (so, one begins from the top left panel and proceeds clockwise). First, in the chromosphere the onset of turbulence does not take place immediately starting from the left foot point: the z^+ spectrum (top left) first shows only the three injected scales

(seen as a red-yellow band), and only very progressively adds smaller scales (first seen as a blue haze). Spatial intermittency then appears about in the middle of the chromosphere in the form of small-scale filamentary structures. This corresponds to a travel time $\Delta L/V_a^0 \simeq 1100$ s, which is close to the nonlinear time $t_{NL}^0 \simeq 800$ s.

In the corona (top panels) one sees in contrast no large parallel gradients, as seen previously with the rms z^+ and z^- energies. A conspicuous feature of the coronal spectrum is the hump appearing as a red ribbon that is displaced towards large scales (when compared to the peak in the chromospheric injected spectrum, top left). This again reveals the inverse transfer already noted above in Fig. 6.

Finally, one sees in the bottom left panel that the wave leaking from the corona makes the z^- chromospheric spectrum look much more developed than its z^+ counterpart.

4.3. The three-layer model: increasing turbulence

We now increase in the three-layer model the turbulence strength χ_0 from 0.04 to 4.8 (runs A, D, F, H). This is achieved by decreasing the nonlinear time, while the leakage time is fixed. Even though we have already seen that the nonlinear time is clearly a strong lower bound for the dissipative time, again, one should thus expect the open model to match the closed model in the limit $\chi_L \gg 1$ at some point. This point is considered again in the discussion where the properties of all models are summarized.

In Fig. 9 we illustrate how the dynamics change in the open three-layer model when increasing χ_0 . The left panel shows the rms magnetic field amplitude in the corona normalized to b_0 , the linear zero-frequency solution, while the two other panels show the (space and time averaged) total energy spectra respectively in the chromosphere and the corona.

The main points are (1) when the nonlinear time is too large (very small χ_0 , run A), one sees that turbulence has no time to develop before reaching the corona. Both the chromospheric and coronal spectra remain largely devoid of small scales. Dissipation is thus negligible. The asymptotic level of the magnetic field is close to its 15 G linear value, the growth of b_{rms} being extremely regular and devoid of any small-scale fluctuations. All this happens in a leakage time. (2) Decreasing the nonlinear time progressively decreases the asymptotic coronal field. Its growth becomes now chaotic, the signal in the lefthand panel showing a whole spectrum of frequencies, with, most remarkably, periods close to the leakage time for the two intermediate values of χ_0 , but also periods close to two chromospheric crossing time $2t_a^{ch} = 1/3t_L$ for the strongest χ_0 (run H in the left panel, see for example the range $t/t_L \in [3, 4]$). (3) At reasonably large χ_0 , the coronal spectra are developed. However, the chromospheric spectra are significantly steeper. In the chromosphere, the slope is close to 1.8, while it is close to 1.7 in the corona. (4) The chromospheric spectra are devoid of the humps that appear in the coronal spectra.

We thus conclude that too weak a cascade does not change linear zero-frequency results at all, and that there is a χ_0 threshold above which turbulence has common properties. There are slight differences in the chromosphere and corona, the main ones being the large-scale coronal peak, and a slightly different slope.

We now examine frequency spectra. We computed frequency spectra of $(z_{rms}^\pm)^2$ at each position along the loop and then they were averaged separately in the corona and in the chromosphere. The original time series was windowed with the hanning procedure, and the zero frequency is also displayed as the lowest frequency in the plot (Fig. 10). The coronal z^+ and z^- have

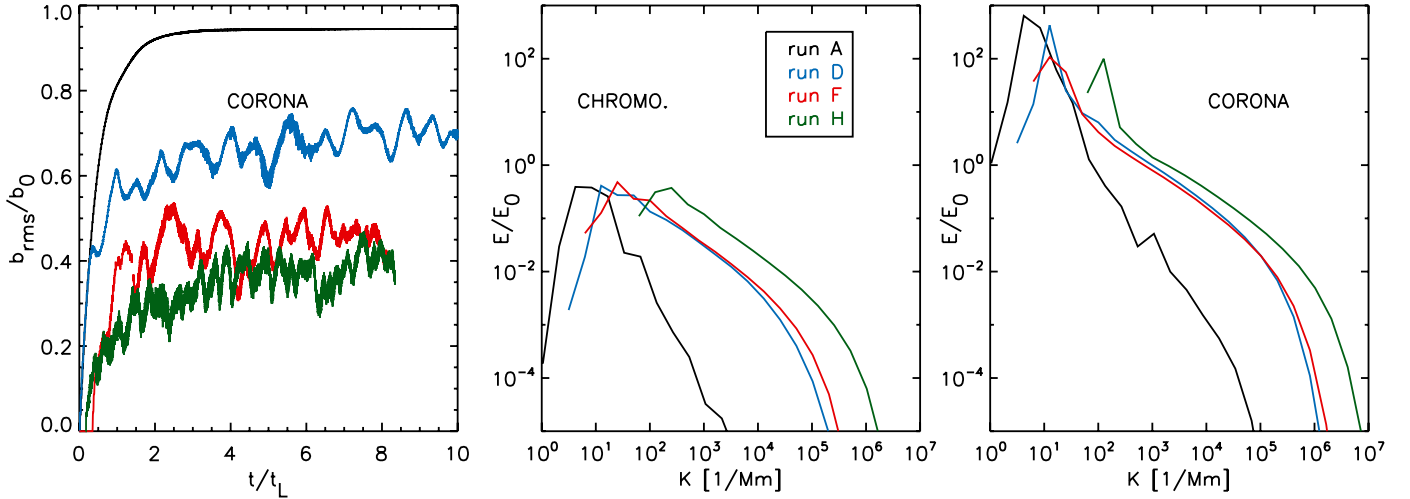


Fig. 9. Runs A, D, F, and H with increasing χ_0 . Left panel: growth of rms coronal magnetic field (normalized to its asymptotic linear value $b_0 = 15$ G). Middle and right panels: total energy spectrum $E(k)$ averaged in time and space in the chromosphere and in the corona, respectively.

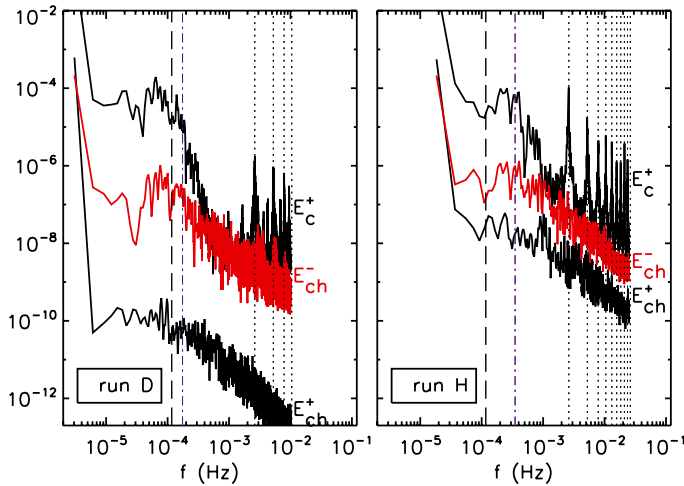


Fig. 10. Runs D and H (weak and strong χ_0): frequency energy spectra $E^+(f)$, $E^-(f)$, computed by taking the Fourier transform of the $(z_{\text{rms}}^\pm(t))^2$ at each plane and then space averaging separately in the chromosphere (bottom black and red lines) and corona (top black line). The E^- (not plotted) and E^+ coronal spectra are indistinguishable. The vertical lines mark some relevant timescales: dotted lines for the resonances at $n \geq 1$; dot-dashed lines for the (round-trip) chromospheric crossing time, $2t_a^{\text{ch}}$; and long-dashed lines for the leakage time, t_L .

practically the same spectrum, so we only plot z^+ in the corona, while the chromospheric spectra are plotted for both z^+ and z^- .

On the coronal spectra peaks appear close to (but not coinciding exactly with) the resonant frequencies: n/t_a^c . This confirms again that the quasi-linear trapping properties are not strongly affected by leakage.

For weak turbulence (left panel), the spectra are dominated by the lowest frequencies, the input zero-frequency and a low-frequency bump. As the strength of turbulence is increased (right panel), more energy goes into finite-frequency resonances, some of them becoming as energetic as the low-frequency part of the spectrum. The location of the low-frequency bump corresponds roughly to two characteristic timescales, the leakage time, t_L , and two chromospheric crossing time, $2t_a^{\text{ch}}$, which we interpret as the signature of the turbulence activity in the coronal and

chromospheric layer, respectively. In run D (low turbulence) two distinct bumps appear in the chromospheric spectrum E_{ch}^+ at frequencies $1/t_L$ and $1/2t_a^{\text{ch}}$, while in run H (strong turbulence) the bump lies between them. In the coronal spectra (and also in E_{ch}^-) the bump is somewhat wider, possibly showing a coupling with the (zero and finite frequency) resonances. The importance of both timescales points out that the low-frequency spectrum in the three-layer model is affected by the coupling between the coronal and chromospheric turbulence.

5. Discussion

We have studied the problem of heating coronal loops by forcing a photospheric shear through the injection of Alfvén waves at one foot point and by waiting for the injected Alfvén waves to be transmitted into the corona, to be trapped (amplified), and finally to dissipate due to turbulence. For this we used a simplification of the RMHD equations that exploits shell models to account for the perpendicular nonlinear coupling.

In contrast to previous work, we considered a finite Alfvén speed difference between the photosphere and the corona and freely propagating waves deep in the photosphere, thus allowing energy to leak back to the chromosphere and to deeper layers of the solar atmosphere. We found that, although leakage does not dramatically change the quasi-linear trapping properties of the corona or the spectral properties of turbulence, it strongly alters the level of the energy trapped in the corona and the resulting dissipation.

We have seen that the coronal energy and dissipation rate vary, depending (i) on the ratio χ_0 of the linear Alfvén crossing time by the nonlinear input time t_{NL}^0 and (ii) on the choice of the atmosphere model, allowing or not the development of a chromospheric turbulence. We now systematically present these variations and discuss them. We present the closed model, one-layer and the three-layer models on an equal footing. The closed model results should allow direct comparison with earlier work, and the comparison between the one-layer and three-layer models should make the effect of chromospheric turbulence clear. However, we consider that the three-layer model is the most realistic of the three models. We vary χ_0 while fixing the Alfvén speed contrast to $\epsilon = 0.02$ and the loop length to $L_c = 6$ Mm. The dependence on ϵ and L_c will be postponed to a further study.

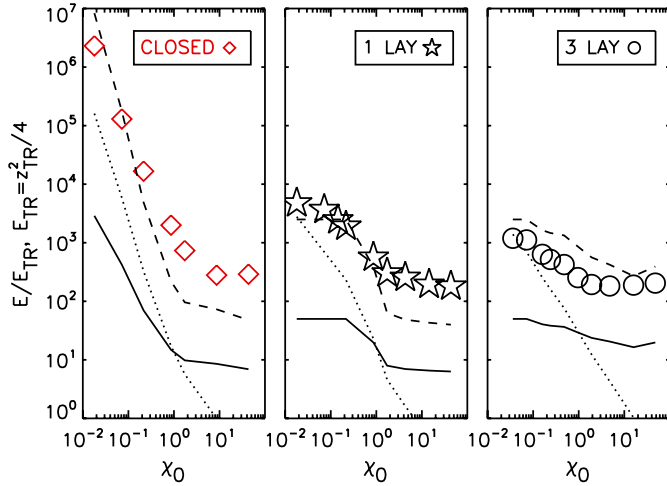


Fig. 11. Coronal energy per unit mass normalized by the T.R. injection energy as a function of the time ratio χ_0 . *Left*: closed model results (symbols); *mid panel*: one-layer model results (symbols); *right*: three-layer model results (symbols); dashed line: resonant scaling; dotted line: intermediate correlation time scaling; solid line: small correlation time scaling.

5.1. Energy

We show in Fig. 11 how the energy trapped in the corona depends on the turbulence strength χ_0 in the different models (left: closed model; midpanel: one-layer; right: three-layer). In each case, we show how the results are fitted by the generalization of the Hollweg-NMV model as given by the three different possible regimes (Eqs. (43)–(45)). For this purpose we normalize the energy to the coronal input energy $z_{\text{TR}}^2/4$, which coincides with the input energy U_0^2 in the closed and one-layer model, while it is a measured quantity for the three-layer model ($z_{\text{TR}}^2 \equiv |z_1^+|^2$ in Fig. 2).

The regime is identified by the choice of the correlation time of the input spectrum, which is different in the different models. For instance, a constant signal in the closed model is a particular case of the resonant regime (line spectrum) while the flat spectrum should be found for a very short correlation time. It is striking that the best fit, although largely imperfect, is always obtained by the resonant expression (zero-frequency spectrum), regardless of the turbulence strength (i.e. both for small and large χ_0).

The behavior of the system is therefore dominated by the $n = 0$ resonance. This could be expected for the closed and one-layer models, since the input signal is time independent, but less so for the three-layer model, in which the chromospheric turbulence modifies the input frequency spectrum to the corona, at least for large χ_0 . It therefore seems that the dominance of the low frequencies is not caused by the particular forcing chosen here, but is a consequence of the coronal activity itself. As we have seen, the coronal spectrum shows a bump at large perpendicular scales containing very low frequencies but this bump is not present in the chromospheric spectrum (see Fig. 9).

A last point concerns the model differences. While all three models attain the same energy level for $\chi_0 > 1$, it is seen that they strongly differ in the weak turbulence regime. In the closed model the energy grows until turbulence becomes efficient enough to balance the input energy. In the opened models, instead, the energy accumulation is prevented by the leakage and the resulting level is much lower.

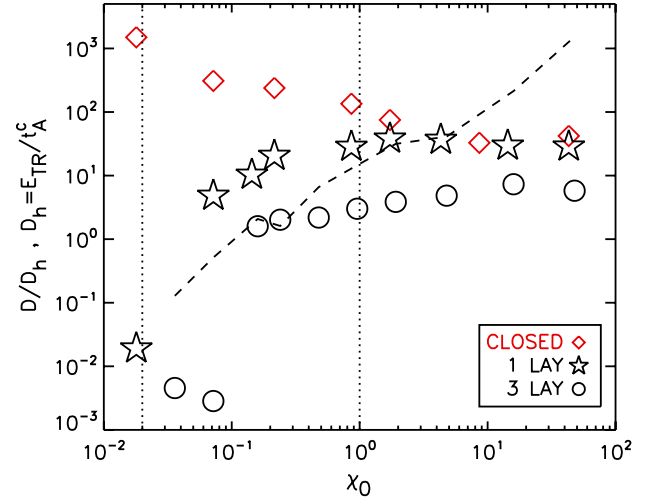


Fig. 12. Dissipation normalized by Eq. (46) vs. χ_0 for the three models. The vertical dotted lines mark the values $\chi_0 = \epsilon(t_{\text{NL}}^0 = t_L)$ and $\chi_0 = 1$. The dashed line is the prediction from Eq. (51) for the three-layer model.

5.2. Heating rate

The heating rate is shown in a single plot for all three models in Fig. 12. We show the dissipation per unit mass normalized to Hollweg expression, $D_h = E_{\text{TR}}/t_a^c$, (Eq. (46)) vs. χ_0 : diamonds are for the closed model, stars for the one-layer model, and circles for the three-layer model.

In the weak turbulent part of the diagram ($\chi_0 < 1$), we again find the same ordering of the models observed above for the energy: a line-tied model leads to a heating rate inversely proportional to the turbulence strength (our results follow the fit $D \propto (u^2/t_a^c)\chi_0^{-1/2}$ proposed by Dmitruk & Gomez 1999), while for the open models the heating rate goes down proportionally to the turbulence strength. We note, however, the sudden drop in the dissipation rate at very low χ_0 (roughly corresponding to $t_{\text{NL}}^0 > t_L$), due to the absence of formation of a high-wave number spectrum in the open models: the coronal energy level is too low to trigger a cascade before fluctuations leak out of the corona.

In the strong turbulent regime ($\chi_0 > 1$), the dissipation is nearly independent of the turbulence strength. The level of this plateau is common to the closed and one-layer models, which differ only in their boundary conditions, but it is lower for the three-layer model. This is to be attributed to the chromospheric turbulence that reduces the coronal input, hence the actual strength of the turbulence, for given χ_0 .

5.3. Dissipation time

Finally we consider in Fig. 13 the dissipation time, $t_D = E/D$, normalized to the coronal crossing time t_a^c . For the open models, the right vertical axis also shows the dissipation time normalized to the leakage time, which makes sense since the ratio ϵ between the Alfvén and leakage time remains fixed in the data shown here. The few points of the open models with very low turbulence strength χ_0 show very high values of the dissipation time, due to the undeveloped turbulence, as already mentioned above.

These points aside, one sees that increasing χ_0 (i.e., decreasing the input nonlinear time), the dissipation time decreases as expected, but that, most remarkably, it stops decreasing when χ_0

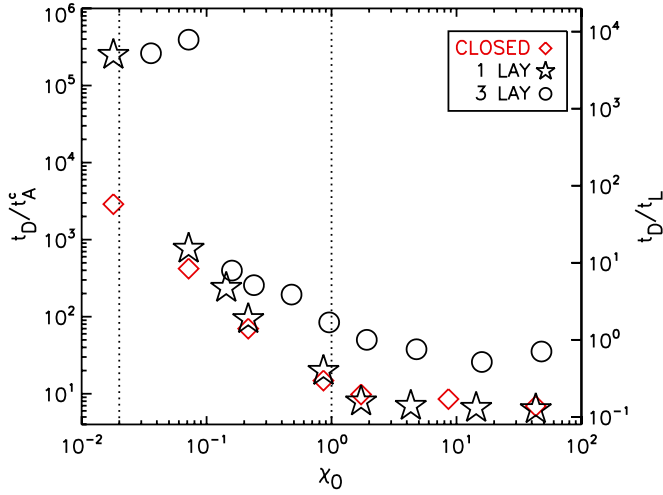


Fig. 13. Dissipation time vs. χ_0 for the three models; note the different normalization in the left and right axis. The vertical dotted lines mark the values $\chi_0 = \epsilon$ ($t_{NL}^0 = t_L$) and $\chi_0 = 1$.

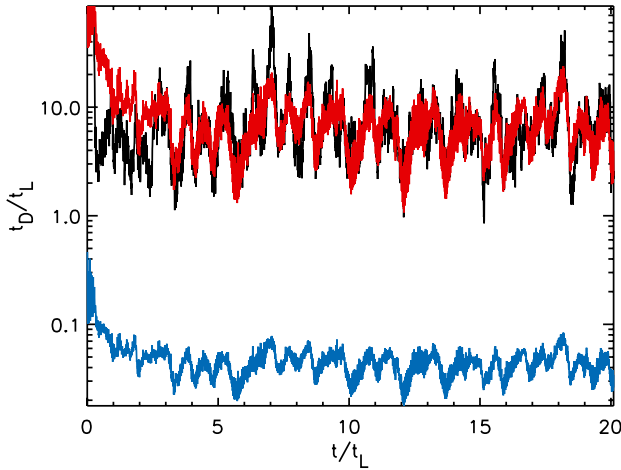


Fig. 14. Run D: comparing the instantaneous dissipation time with the slow Iroshnikov-Kraichnan timescale (red) and the standard nonlinear time (blue, below).

reaches about unity. The plateau is comparable for the one-layer and closed models, corresponding to $t_L \simeq 10t_D$ in the one-layer model, while it corresponds to $t_L \simeq t_D$ in the three-layer model.

It would certainly be progress, both from the theoretical and the practical viewpoints, to understand how the heating time and energy are related. The difficulty is that the usual relations here are modified by the existence of the large-scale hump in the spectrum. One cannot consider that there is a straightforward (direct) cascade from the large to the small scales, since the energy is clearly “blocked” at large scales.

That this is so can be easily verified by comparing the instantaneous dissipation time with the nonlinear time $t_{NL} = 1/(ku)$ (with $k = k_\perp$ the largest forcing scale, and u the rms velocity), which usually rules the direct Kolmogorov cascade. However, a strikingly good result (shown in Fig. 14) is obtained when using a factor V_a^c/u to increase the nonlinear time $1/(ku)$:

$$t_D \simeq 1/(ku)(V_a^c/u). \quad (49)$$

The fit is good enough and works for all values listed in Table 1 for the turbulence strength χ_0 for the three-layer model.

However, the fit is more hazardous for the one-layer model, and simply does not work at all for the closed model.

This simple law for the three-layer model deserves some comment. The expression in Eq. (49) recalls the delayed cascade time predicted by the Iroshnikov-Kraichnan phenomenology. This phenomenology was meant to describe the (delayed) cascade of interacting Alfvén waves with wavevectors not perpendicular to the mean field. The delaying effect was supposed to work all along the cascade, leading to a specific spectrum, different from the Kolmogorov one (3/2 instead of 5/3). Here, the situation is different. Indeed, the coronal spectrum adopts a slope close to 5/3, not 3/2, and, most probably (but this study is postponed to a later work), the characteristic timescale that rules the cascade here is the strong turbulence timescale $1/(ku)$. However, the energy is dominated by the spectral hump at large scale, which is not ruled by the fast timescale, but by the delayed timescale of Eq. (49). This comes from the effect of the resonant trapped linear modes that act to deplete the nonlinear coupling terms, in the same way as in the Iroshnikov-Kraichnan phenomenology, although only at large scales.

5.4. Conclusion

We focus here on the three-layer model, which is by far the most realistic model of the three we have studied. We have increased our knowledge concerning the physical mechanisms at work since we know now that a) the coupling between the chromospheric input and that of the coronal cavity is close to that of zero-frequency resonance, b) leakage always plays a substantial role, and c) the timescale of dissipation is long because the Kolmogorov time $1/(ku)$ is reduced by the u/V_a^c factor.

We also found that a rough prediction for the dissipation rate is given by the classical expression, $D \simeq D_H = z_{TR}^2/t_a^c$ (Eq. (46), see Fig. 12), where z_{TR} is the amplitude of the input fluctuation at the T.R. level. This result is a bit paradoxical, since this relation was first obtained by Hollweg, on the basis of assumptions that are not verified in our simulations: (i) a short correlation time for the chromospheric input and (ii) negligible leakage. In our simulations the conditions are completely different: (i) long correlation time (ii) and substantial leakage. The solution to the paradox lies in the rough compensation of several effects: (i) the energy level is decreased by leakage and the chromospheric turbulence, but largely increased by resonance; and (ii) the dissipation time is increased by the large-scale hump.

Although the above heating rate contains the unknown T.R. level of input fluctuations, it can be used as a predictive law if we identify the T.R. input value z_{TR} with the (imposed) photospheric value U_0 . This gives the simple classical result

$$D = D_{H0} = U_0^2/t_a^c. \quad (50)$$

If we again consider the three-layer results and plot the ratio D/D_{H0} instead of the ratio D/D_H as in Fig. 12, it is interesting to note that the result is not basically changed, but nevertheless the deviation from the horizontal (here $D/D_{H0} = 1$) is reduced a bit, because limited to at most a factor 5.

Can we use our new knowledge to improve the prediction of the dissipation rate beyond the approximate law $D \simeq D_H$? Unfortunately the answer is no, because of our poor knowledge of the relation between the known photospheric input U_0 and the (largely unknown) chromospheric input z_{TR} , as well as the coronal velocity fluctuation level u_c . If we bypass this step by replacing the unknown quantities (z_{TR}, u_c) by U_0 , using the zero-frequency resonant expressions with dominant leakage for the

coronal fluctuations ($b_c = U_0/\epsilon$, $u_c = U_0$, Eq. (45)) and the dissipation time (Eq. (49)), we obtain for the dissipation rate per unit mass:

$$D = b_c^2/t_D \approx U_0^2/\epsilon^2(1/t_{NL}^0)(U_0/V_a^c) \\ = D_H (L/l_\perp) (U_0/V_a^0)^2. \quad (51)$$

When using this expression with the parameter values of the three-layer model as given in Table 1, one obtains the dashed line in Fig. 12. This is clearly not an improvement on the simple relation $D/D_H \approx 1$. It is actually much worse by direct comparison with the numerical simulation results (the circles in Fig. 12) but also from a more general point of view, since dissipation is largely believed to grow with B_0 , while Eq. (51) predicts the reverse ($D \propto 1/V_a^0$).

To progress, we must understand how to relate the chromospheric and coronal velocity level to the photospheric one. We should also explore how the heating rate depends on all parameters, in particular, the Alfvén speed contrast ϵ and the loop length L_c . Finally, we should investigate whether the properties of photospheric turbulence, in particular the correlation time, modifies the coronal reaction.

Acknowledgements. We benefited from useful discussions with G. Belmont. A.V. acknowledges support from the Belgian Federal Science Policy Office through the ESA-PRODEX program. The research described in this paper was carried out in part at the Jet Propulsion Laboratory, California Institute of Technology, under a contract with the National Aeronautics and Space Administration.

Appendix A: Atmospheric model

To obtain the parameter χ_0 for a “realistic” coronal loop, we have to determine the Alfvén crossing time, in other words, the relation $\epsilon(L)$ for a given V_a^0 . We model the loop as a semicircular cylinder of radius R , subject to a constant vertical acceleration $g = GM_\odot/R_\odot^2$. The loop has constant cross-section and is threatened by a uniform magnetic field. For simplicity the loop is assumed to be isothermal in the chromosphere and in the corona. The two temperatures are related by the jump at the transition region (T.R.)

$$T(s) = T_0 + \frac{1}{2} (T_c - T_0) \left[\tanh\left(\frac{s - s_{tr}^R}{\delta_{tr}}\right) + \tanh\left(\frac{s_{tr}^L - s}{\delta_{tr}}\right) \right] \quad (A.1)$$

where $s \in [0, \pi R]$ is the coordinate along the loop, $s_{tr}^{L,R}$ and δ_{tr} are the position and width of the two transition regions, $s_{tr}^L = R \sin^{-1}(h_{tr}/R)$, $s_{tr}^R = L - s_{tr}^L$. We set the T.R. height $h_{tr} = 2$ Mm and its width to $\delta_{tr} = 0.2$ Mm. We consider two coronal temperatures, $T_c = 0.8$ MK, 3 MK in order to consider short loops (reaching the low corona) and longer loops. We finally assign the following values to the “base” parameters, magnetic field, number density, and temperature: $B_0 = 100$ G, $n_0 = 10^{17}$ cm $^{-3}$, and $T_0 = 4500$ K.

The density profile along the loop is obtained by solving the equation for the static equilibrium

$$\frac{1}{\rho} \frac{d\rho}{ds} = -\frac{1}{T} \frac{dT}{ds} - \frac{g}{T} \cos \pi s/L, \quad (A.2)$$

and the \cos function accounts for the projection of gravity along the loop. Varying the loop length we find *short* loops that do not reach the T.R. heights ($R < 2$ Mm) and *long* loops that indeed reach the corona. For the former, the density is found by direct integration of the above equation, while the equations will be solved numerically for long loops.

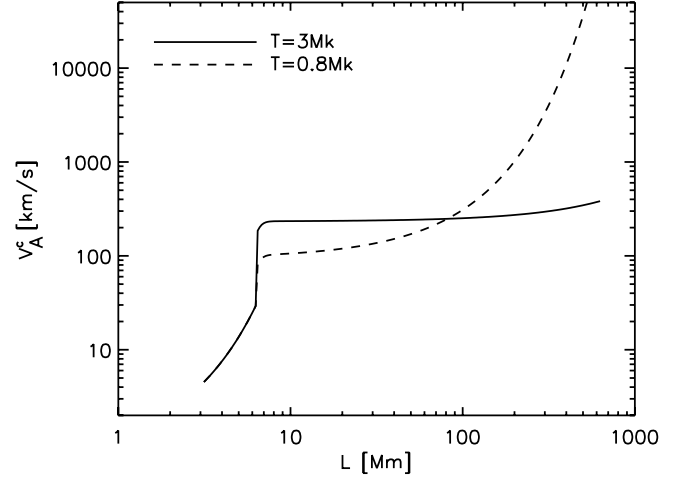


Fig. A.1. Coronal Alfvén speed V_a^c as a function of the loop length L for the hydrostatic two-temperature model of a coronal loop. Solid and dashed lines correspond to coronal temperatures of 3 MK and 0.8 MK, respectively.

The static loop model, according to its temperature profile, defines a relation $\epsilon(L)$ that can be estimated by considering the temperature jump at the T.R. as a discontinuity and calculating the density at the loop apex $s = L/2$. By integrating from the photosphere to the T.R. and from the T.R. to the corona, one finds

$$\ln(\rho_{tr-}/\rho_0) = -gh_{tr}/T_0 \quad (A.3)$$

$$\ln(\rho_c/\rho_{tr+}) = -g(R - h_{tr})/T_c \quad (A.4)$$

where $\rho_{tr\pm}$ are the densities just below and above the transition region. Assuming that the T.R. is in pressure equilibrium, the density jump is given by $\ln(\rho_{tr+}/\rho_{tr-}) = \ln(T_0/T_c)$ so finally one gets

$$2 \ln \epsilon = -\left[\frac{R - h_{tr}}{H_c} + \frac{h_{tr}}{H_0} \right] + \ln \left[\frac{T_0}{T_c} \right] \approx -\left[\frac{h_{tr}}{H_0} \right] - \ln \left[\frac{T_c}{T_0} \right] \quad (A.5)$$

where we have introduced the density scale heights in the chromosphere and corona, $H_0 = T_0/g \approx 0.27$ Mm and $H_c = T_c/g \approx 60$ Mm respectively, and make use of the definition $\epsilon = (\rho_c/\rho_0)^2$. From Eq. (A.5) one can see that for long loops, $R < H_c$ (used in the last equality), the density contrast is determined almost entirely by the T.R. jump and is *independent* of the loop length, except for very long loops that span a density scale height in the corona ($L \gg 200$ Mm). By numerical integration of Eqs. (A.1), (A.2) we obtain for a long loop $\epsilon = 0.004$, which is a factor two larger than the estimate based on Eq. (A.5), the discrepancy arising from the fact that the T.R. is not in pressure equilibrium.

To obtain the solid and dashed black lines in Fig. 3, we use the relation $\epsilon(L) = V_a^0/V_a^c(L)$ as found from the numerical integration for the two coronal temperatures $T_c = 0.8$ MK and $T_c = 3$ MK (here $V_a^c(L) \equiv \max_x[V_a(L, x)]$). The maximal Alfvén speed is shown in Fig. A.1 as a function of the loop length: V_a^c increases monotonically and then experiences a sudden jump at around $L = 4.2$ Mm. After that jump it decreases slightly and then increases again monotonically. In the first part ($L \lesssim 4.2$ Mm), loops are short enough to remain in the first isothermal layer (the chromosphere), where the density scale height is small. The jump at $L \approx 4.2$ Mm is determined by the fact that loops reach the height of the T.R. In this thin

layer, the density scale height is very small, and density drops very quickly. Loops with length between ≈ 4.2 Mm and 4.4 Mm do not penetrate the corona, remaining in the T.R., so the Alfvén speed increases even more, reaching a local maximum. The next part of the profile is characteristic of loops that reach the second isothermal layer (the corona), where the density scale height is large.

References

- Biskamp, D. 1994, *Phys. Rev. E (Statistical Physics)*, 50, 2702
- Buchlin, E., & Velli, M. 2007, *ApJ*, 662, 701
- Dmitruk, P., & Gomez, D. O. 1999, *ApJ*, 527, L63
- Dmitruk, P., Gómez, D. O., & Matthaeus, W. H. 2003, *Phys. Plasm.*, 10, 3584
- Giuliani, P., & Carbone, V. 1998, *Europhys. Lett.*, 43, 527
- Gloaguen, C., Léorat, J., Pouquet, A., & Grappin, R. 1985, *Phys. D Nonlinear Phenom.*, 17, 154
- Grappin, R., Aulanier, G., & Pinto, R. 2008, *A&A*, 490, 353
- Hollweg, J. V. 1984, *Sol. Phys.*, 91, 269
- Ionson, J. A. 1982, *ApJ*, 254, 318
- Malara, F., Nigro, G., Onofri, M., & Veltri, P. 2010, *ApJ*, 720, 306
- Milano, L. J., Gomez, D. O., & Martens, P. C. H. 1997, *ApJ*, 490, 442
- Nigro, G., Malara, F., Carbone, V., & Veltri, P. 2004, *Phys. Rev. Lett.*, 92, 194501
- Nigro, G., Malara, F., & Veltri, P. 2005, *ApJ*, 629, L133
- Nigro, G., Malara, F., & Veltri, P. 2008, *ApJ*, 685, 606
- Ofman, L. 2002, *ApJ*, 568, L135
- Parker, E. N. 1972, *ApJ*, 174, 499
- Rappazzo, A. F., Velli, M., Einaudi, G., & Dahlburg, R. B. 2007, *ApJ*, 657, L47
- Rappazzo, A. F., Velli, M., Einaudi, G., & Dahlburg, R. B. 2008, *ApJ*, 677, 1348
- Strauss, H. R. 1976, *Phys. Fluids*, 19, 134